Thermal inertia of main belt asteroids smaller than 100 km from IRAS data

Marco Delbo, Paolo Tanga

Thermal inertia of main belt asteroids smaller than 100 km from IRAS data

Marco Delbo' *,[1] and Paolo Tanga

Laboratoire Cassiopée, Observatoire de la Côte d'Azur

BP 4229, 06304 Nice cedex 04, France.

Abstract

Recent works have shown that the thermal inertia of km-sized near-Earth asteroids (NEAs) is more than two orders of magnitude higher than that of main belt asteroids (MBAs) with sizes (diameters) between 200 and 1,000 km. This confirms the idea that large MBAs, over hundreds millions of years, have developed a fine and thick thermally insulating regolith layer, responsible for the low values of their thermal inertia, whereas km-sized asteroids, having collisional lifetimes of only some millions years, have less regolith, and consequently a larger surface thermal inertia.

Because it is believed that regolith on asteroids forms as a result of impact processes, a better knowledge of asteroid thermal inertia and its correlation with size, taxonomic type, and density can be used as an important constraint for modeling of impact processes on asteroids. However, our knowledge of asteroids' thermal inertia values is still based on few data points with NEAs covering the size range 0.1–20 km and MBAs that >100 km.

Here, we use IRAS infrared measurements to estimate the thermal inertia values of MBAs with diameters <100 km and known shapes and spin vector: filling an important size gap between the largest MBAs and the km-sized NEAs. An update

Preprint submitted to Planetary and Space Science *6 August 2008*

to the inverse correlation between thermal inertia and diameter is presented. For some asteroids thermophysical modelling allowed us to discriminate between the two still possible spin vector solutions derived from optical lightcurve inversion. This is important for (720) Bohlinia: our preferred solution was predicted to be the correct one by Vokrouhlický et al. (2003, Nature 425, 147) just on theoretical grounds.

Key words: Asteroids, Near-Earth Objects, Infrared observations

1 Introduction

Thermal inertia is a measure of the resistance of a material to temperature change. It is defined by $\Gamma = \sqrt{\rho\kappa c}$, where κ is the thermal conductivity, ρ the density and c the specific heat. Γ is a key parameter that controls the temperature distribution over the surface of an asteroid. In the limit of zero thermal inertia the surface of an asteroid is in instantaneous equilibrium with the solar radiation and displays a prominent temperature maximum at the sub-solar point. In the realistic case of a rotating asteroid with finite thermal inertia the temperature distribution becomes more smoothed out in longitude with the afternoon hemisphere hotter than the morning one (see e.g. Delbo' and Harris, 2002; Delbo' , 2004; Mueller , 2007, and references therein).

Acquisition of temperature data (e.g. from thermal infrared observations at different wavelengths around the body's heat emission peak) over a portion of the diurnal warming/cooling cycle can be used to derive the thermal inertia

* Corresponding author.
Email address: delbo@obs-nice.fr (Marco Delbo').
[1] Supported by the European Space Agency (ESA). Also at INAF, Astronomical Observatory of Torino, Italy.

of planetary surfaces by fitting a temperature curve calculated by means of a thermal model to the observed data. Asteroids surface temperatures depend also on the bodies' shapes, inclination of their spin axis and rotation rates. For those objects for which this information is available the so-called thermophysical models (TMPs) can be used to calculate infrared fluxes as function of the asteroid's albedo, thermal inertia and macroscopic roughness. Those parameters are adjusted until best fit to the data is obtained (see Mueller , 2007, and §2 for details)

Knowledge of the thermal inertia of asteroid surfaces is important for several reasons:

(1) thermal inertia is a sensitive indicator for the presence or absence of thermally insulating loose material on the surface such as regolith or dust (see e.g. Christensen et al., 2003). The value of Γ depends on regolith depth, degree of induration and particle size, rock abundance, and exposure of solid rocks and boulders within the top few centimeters of the subsurface (i.e. a few thermal skin depths). Typical values of Γ in (S.I. units J m^{-2} $s^{-0.5}$ K^{-1}) are 30 for fine dusts, 50 for the lunar regolith, 400 for coarse sands (note that a thermal inertia of 400 for coarse sand assumes the presence of some atmosphere, even if as thin as the Martian one), and 2500 for bare solid rocks (Mellon et al. , 2000; Spencer et al., 1989; Jakosky, 1986, see also http://tes.asu.edu/TESworkshop/Mellon.pdf). Information about thermal inertia is therefore of great importance in the design of instrumentation for lander missions to asteroids such as the Marco Polo of the European Space Agency, because it allows one to have information about the soil and sub–soil temperatures and the make up of asteroid surfaces.

(2) The presence or absence and thickness of the regolith on km–sized bodies can give hints about the internal structure of asteroids: recent work by Michikami et al. (2007) showed that small asteroids (with sizes $\sim$1 km) can capture collisional debris and build up regolith if their tensile strength is not high;

(3) Thermal inertia affects the strength of the Yarkovsky effect (see Bottke et al., 2006, and references therein) which is responsible for the gradual drifting of the orbits of km-sized asteroids and is thought to play an important role in the delivery of near-Earth asteroids (NEAs) from the main belt (Morbidelli and Vokrouhlický , 2003), and in the dynamical spreading of asteroid families (see Bottke et al., 2006).

(4) Understanding asteroid thermal inertia is important to estimate and reduce systematic errors on sizes and albedos of asteroids, when the these are determined by means of simple thermal models such as the Standard Thermal Model (STM; Lebofsky and Spencer , 1989) neglecting the effect of the rotation of these bodies and their thermal inertia (Delbo' and Harris, 2002; Delbo' , 2004).

To date the value of the thermal inertia has been derived for seven large main-belt asteroids (MBAs) (Müller and Lagerros, 1998; Müller and Blommaert, 2004; Mueller et al. , 2006) and six NEAs (Harris et al., 2005, 2007; Mueller et al. , 2004; Mueller , 2007; Müller et al., 2004). Moreover, the mean value of Γ was estimated for the NEAs with multiwavelength thermal infrared data, the latter believed to be representative of the thermal inertia of NEAs with sizes between 0.8 and 3.4 km (Delbo' et al., 2007).

By comparing MBA and NEA thermal inertia values, an inverse correlation between Γ and asteroid diameter D was derived (Delbo' et al., 2007) of the form:

$$\Gamma = d_0 D^{-\xi}, \tag{1}$$

where D is the diameter of a sphere with a volume equivalent to that of the asteroid shape. Equation 1 has also important consequences for the Yarkovsky effect, implying that that the orbital semimajor axis drift rate of MBAs due to the Yarkovsky effect is proportional to $\sim D^{\xi-1}$ (Delbo' et al., 2007) rather than to D^{-1}, the latter being the expected dependence for size independent thermal inertia. Given the small number of determined asteroid thermal inertia values, Delbo' et al. (2007) used a unique value for ξ and d_0 across an interval of 4 orders in magnitude in D. Their best-fit values are $\xi = 0.48 \pm 0.04$ and $d_0 = 300 \pm 47$, where D is km and Γ in S.I. units (J m^{-2} s$^{-0.5}$ K^{-1}).

However, there are several reasons to suspect that surface properties of large asteroids may be different from those of smaller bodies. In this case ξ might acquire different values in different size ranges. For example, Bottke et al. (2005) showed that asteroids with D >100 km and most bodies with D >50 km in size are likely to be primordial objects that have not suffered collisional disruption in the past 4 Gyr. These objects have resided in the asteroid belt long enough to build up a fine regolith to cause their low Γ–values regardless of their size. Moreover, the same work has shown that objects smaller than ~30 km are statistically ejecta from the catastrophic collisional disruption of larger parent bodies. In the latter case, the more recent the smaller is an object. The surfaces of these asteroids might be systematically fresher with less mature and less thick regolith, implying higher–Γ values. At the smaller end of the size distribution, an unknown role might be played by the YORP effect. By increasing the rotation rate of these bodies, regolith might have been ejected from the surfaces, leading to large Γ–values. Furthermore, our knowledge of Γ for asteroids <20 km in size is based on NEAs only. While it is believed that NEA surfaces are representative of the small ($D < 20$ km) MBA surfaces, this has still to be demonstrated. Some NEAs might have suffered planetary close approach strong enough to alter their surfaces, for instance by stripping off some of the regolith (see e.g. Walsh and Richardson, 2006). This is not the case for small MBAs. Furthermore, thermal inertia is a function of temperature ($\Gamma \propto T^{3/2}$; see e.g. Mueller , 2007; Delbo' et al., 2007, for some discussion). This effect may lead to Γ offsets between cooler MBAs and hotter NEAs.

In this work we present new determination of MBA thermal inertia from thermophysical modeling of data obtained by the Infrared Astronomical Satellite (IRAS). We focus on MBAs with $D < 100$ km in order to fill the gap of data between NEAs and the largest MBAs and improve our understating of the relation between thermal inertia and asteroid size.

In §2 we present the method used to derive the thermal inertia of MBAs from IRAS data and the selection of the targets. In §3 we describe the results obtained for each studied asteroid. Furthermore, in §4, we discuss our novel determination of asteroid thermal inertia values in the context of the aforementioned published results.

2 Thermophysical modeling of IRAS data

The Infrared Astronomical Satellites (IRAS) measured the thermal emission of more than 2200 asteroids. Asteroid thermal infrared fluxes measured by IRAS are available through the Planetary Data System on–line archives (Tedesco et al. , 2004). The main goal of the IRAS Minor Planet Survey (IMPS; Tedesco , 1992) was the determination of asteroid sizes. Due to the lack of knowledge of asteroid spin vectors and shapes, asteroid sizes of the IMPS and of its recent revision, the Supplemental IRAS Minor Planet Survey (SIMPS; Tedesco et al. , 2002), were derived by modeling IRAS data with the "refined" Standard thermal model (STM; Lebofsky et al., 1986). The STM assumes spherical, non–rotating bodies. In particular, this model assumes Γ=0, so that it can not be used to empirically constrain the thermal inertia.

However, for ∼70 MBAs, the Asteroid Models from Lightcurve Inversion database (hereafter AMLI, a catalogue of asteroid shapes and spin vector solutions) have been made available recently [2] . These models have been derived solving the inverse problem of determining the object's shape, its rotational state, and the scattering properties of its surface from optical lightcurves using a method developed by Mikko Kaasalainen and colleagues (see Kaasalainen et al., 2002, 2001; Kaasalainen and Torppa, 2001, and references therein).

Theses asteroid shapes and spin vector solutions can be used to perform thermophysical modeling of IRAS data, thereby allowing the derivation of sizes and thermal inertia values.

The thermal inertia of an asteroid can be derived by comparing measurements of its thermal-infrared flux to synthetic fluxes generated by means of a thermophysical model (TPM; Delbo' , 2004; Mueller , 2007, and references therein). A TPM uses the spin vector information to orient a mesh of planar facets (obtained from the AMLI) describing the shape of the asteroid at the time of each thermal infrared measurement. The temperature of each facet is determined by

[2] on the internet at: http://astro.troja.mff.cuni.cz/∼projects/asteroids3D/web.php

numerically solving the one-dimensional heat diffusion equation using presets Γ–values (e.g. 0, 5, 10,...,1000 J m^{-2} s$^{-0.5}$ K^{-1}). Macroscopic surface roughness is modeled by adding hemispherical craters of variable opening angle, γ_C, and variable surface density, ρ_C. Thermal conduction is also accounted for within craters. We used four preset combinations of γ_C and ρ_C spanning the range of possible surface roughness (see table 1). Following the procedure of Mueller (2007), for each roughness model and each value of Γ, the factor a that linearly scales all mesh vertices is determined by the minimization of the function $\overline{\chi}^2 = 1/(N - N_f) \sum_{i=1}^{N} \left(\frac{a^2 f_i' - f_i}{\sigma_i} \right)^2$, where f_i', f_i, and σ_i are the synthetic TPM generated fluxes, the IRAS thermal infrared fluxes and their quoted uncertainties, respectively; N is the number of observations and N_f is the number of the model parameters adjusted in the fit (degrees of freedom). In this work case N_f is always equal to 2, i.e. thermal inertia and D.. The location of the minimum $\overline{\chi}^2$ as function of Γ gives the best–fit asteroid surface thermal inertia for each roughness model. The value of a at Γ–minimum is used to determine the best–fit values of D.

From the AMLI web site, we selected those MBAs with SIMPS diameters <100 km and at least ∼20 IRAS measurements. Each IRAS observation (the so–called sighting) consisted of four simultaneous measurements of the asteroid's thermal infrared flux at 12, 25, 60, and 100 μm. Our list includes (21) Lutetia, (32) Pomona, (44) Nysa, (73) Klytia, (110) Lydia, (115) Thyra, (277) Elvira, (306) Unitas, (382) Dodona, (584) Semiramis, (694) Ekard, and (720) Bohlinia. Flux values for each asteroids are reported in Table 5. Table 2 gives basic information about the physical properties of the objects along with the number of IRAS measurements and the range of observing dates. Table 4 (Supplementary On–line Material) report the AMLI models (donloaded in

December 2007) used in this work.

3 Results

For each object we derived an estimate of the surface thermal inertia from the analysis of the plot of the $\overline{\chi}^2$ as function of Γ for different degree of surface roughness (see §2) [3]. The best–fit values of D are given in table 3 and used in in Fig. 1 to plot Γ vs. D along with thermal inertia values from previous works. For those asteroids for which more than one shape and spin vector solution are available, we determined the one that gives the lowest $\overline{\chi}^2$, which is the solution that we prefer. Our results are particularly important for the asteroid (720) Bohlinia for which our preferred spin state solution was also predicted to be the corrected one just on theoretical grounds by Vokrouhlický et al. (2003, see also §4).

We note that, although shape uncertainties are difficult to be estimated from optical lightcurve inversion and that the constraint of convexity of the shapes from the AMLI data base plays a role in the calculation of the thermal infrared emission of these bodies, our results show that the global approximation of the shapes is in general adequate to provide a good fit of IRAS infrared measurements. However, in the case of of (73) Klytia thermophysical modeling of IRAS data resulted in a poor fit ($\overline{\chi}^2 \sim 8$; 26 data points) independently of the spin vector solution used. We note that recent lightcurve data yield a different spin vector solutions to those reported in the AMLI (A. Carbognani, personal

[3] See the Supplementary On–line Material for a detailed description of TPM results including $\overline{\chi}^2$ plots for each asteroid and each spin vector solution obtained from the AMLI web site.

communication). We leave the detailed investigation of the case of (73) Klytia to a future work.

4 Discussion

This work represents the first attempt of thermal inertia determination of MBAs with sizes $\lesssim$100 km via thermophysical modeling of IRAS data using shapes and spin vectors derived from optical lightcurve inversion. The values derived for the thermal inertia are in general intermediate between those of NEAs and those obtained for the largest MBAs with sizes in the range between 200 and 1000 km.

Figure 1 shows asteroids' thermal inertia values derived from this work along with other values taken from the literature (Delbo' et al., 2007; Harris et al., 2005, 2007; Mueller , 2007; Mueller et al. , 2006, 2004; Müller and Lagerros, 1998; Müller and Blommaert, 2004; Müller et al., 2004) plotted as function of objects' diameter. The thermal inertia of (54509) YORP (the leftmost data point) is a preliminary result from the study of Mueller (2007).

The dashed and the dotted lines of Fig. 1 represent the fit of Eq. (1) to MBAs only and to NEAs only, respectively. Resulting values of ξ are 1.4±0.2 for MBAs and 0.32±0.09 for NEAs. The highly different slopes derived for MBAs and NEAs indicate that a single power law gives a poor fit to the data over the D range 0.1 – 1000 km, in contrast with the results of Delbo' et al. (2007), which where based on a smaller dataset of thermal inertia values. Given the errorbars affecting asteroid thermal inertia determination, the Γ vs D dependence might also be flat for D in the range between 1 and 100 km and might drop for $D > 100$ km down to the low thermal inertia value observed for the largest bodies of the Main Belt. Interestingly, Fig. 1 shows that the NEA power law can reasonably fit well also MBAs with D <100 km (best–fit $\xi = 0.21 \pm 0.04$ for the NEAs and the MBAs with $D < 100$ km). This might be an indication of the different regolith properties that the largest and likely primordial asteroids have in comparison to bodies with D <100 km, the latter probably having been catastrophically disrupted and rebuilt during the age of the solar system.

We checked the thermal inertia values derived by means of our method against values derived by other authors: our estimate of the thermal inertia of (21) Lutetia is in agreement with the Γ–values derived by Mueller et al. (2006), Mueller (2007), and Carvano et al. (2007). We performed thermophysical modeling of IRAS data also for some of the largest MBAs whose shape and spin vector solutions are available in the AMLI web site: for instance, we derived Γ between 5 and 20 J m^{-2} $s^{-0.5}$ K^{-1} for 2 Pallas. This low–Γ value is in agreement with previous determination of the thermal inertia of this object (Spencer et al., 1989; Müller and Lagerros, 1998).

We note that for (720) Bohlinia the first spin solution (λ_p=33.09°, β_p=52.39°, our preferred one) provides a better fit to IRAS data than second the spin solution (λ_p=238.52°, β_p=39.67°). Thermophysical modeling of infrared data allowed us to discriminate between the two still possible spin state solutions obtained by the optical photometry. The first spin solution was predicted to be the correct one by Vokrouhlický et al. (2003) on theoretical grounds: they have shown that spins vectors of the four prograde-rotating Koronis asteroids (including 720 Bohlinia) are trapped in a secular spin-orbit resonance which produces their paralelism in space. On the other hand, in the case of the retrograde rotator (277) Elvira, which also belongs to the Koronis family, our thermophysical analysis of IRAS data can not remove the spin solution degeneracy. However, both spin solution are theoretically possible, as the study of Vokrouhlický et al. (2003) does not put any constraint on the retrograde rotators in the Koronis family. We note also, that due to very low inclination of the Koronis orbits any optical photometry dataset would not be able to distinguish between the two spin orientations, whereas the infrared data have the capability to break this degeneracy.

Table 3 reports the best–fit effective diameters, D, derived by means of our TPM, for each of the studied body. Figure 2 shows the ratio between D and SIMPS diameters as function of D. It can be clearly seen that D–values tend to be larger than SIMPS diameters. Moreover, a correlation between the size of asteroids and the ratio between TPM and SIMPS diameters appears from Fig. 2, such that the deviation between TPM diameters and SIMPS diameters increases for smaller objects. While we caution that the data set is small, this correlation is intriguing and may be indicative of an effect due to the asteroid thermal properties: because we find that Γ increases with decreasing asteroid size, diameters of objects derived under the STM assumption of Γ=0 are less reliable the smaller they are. It is already known that for significant thermal inertia the STM underestimate the real sizes. The correlation we see in Fig. 2 might be due to this fact.

We leave a more detailed investigation of how SIMPS diameters compares with TPM ones and of the accuracy of the latter to a future work devoted to the derivation of sizes and thermal properties of all asteroids in the AMLI database and with IRAS data.

We underline here the potential of our approach: it is expected that shape and spin vector solutions will be derived from optical photometry obtained for instance by the mission Gaia of the European Space Agency for more than 10,000 asteroids (Mignard et al. , 2007), or by ground based surveys such as Pan-STARRS (Durech et al., 2005). Thermal infrared data will be soon available for more than 10,000 asteroids from space missions such as Spitzer, Akari, and WISE (see e.g. the work of Trilling et al., 2007). The combination of the two data sets will enable us to use the TPMs and derive asteroid sizes and surface thermal inertia valuesdown to diameters of few km in the main belt.

5 Conclusions

We derived the thermal inertia values of 10 main belt asteroids in the size range between 30 and 100 km from thermophysical modeling of IRAS data. Our results indicate that thermal inertia increases with decreasing size more rapidly for main belt asteroids with diameters between 30 and 1000 km than for near-Earth asteroids smaller than 30 km. This might reflect the different regolith properties between the largest, likely primordial asteroid and the smaller ones, catastrophically disrupted and rebuilt during the age of the solar system. We also discuss the comparison between diameters from thermophysical modeling of IRAS data and SIMPS diameters for the asteroids included in this study.

Acknowledgments

The work of Marco Delbo has been carried out in the framework of the European Space Agency (ESA) External Fellowship Program. Part of this research was also carried out while he was a Henri Poincaré Fellow at the Observatoire de la Côte dAzur. The Henri Poincaré Fellowship is funded by the CNRS-INSU, the Conseil Général des Alpes-Maritimes and the Rotary International – District 1730.

We thank the referees David Vokrouhlický and Michael (Migo) Mueller for suggestions that led to significant improvements of the manuscript. M.D. wishes also to acknowledge fruitful discussions with Ed Tedesco. The thermophysical model was mainly run on a Opteron 8–processors computer (thot) at the Observatoire de la Côte d'Azur dedicated to the Gaia space mission.

References

Bottke,W.F., Durda, D.D., Nesvorný, D., Jedicke, R., Morbidelli, A., Vokrouhlický, D., Levison, H.F., 2005. Linking the collisional history of the main asteroid belt to its dynamical excitation and depletion. Icarus 179, 63–94.

Bowell, E., Hapke, B., Domingue, D., Lumme, K., Peltoniemi, J., Harris, A.W. 1989. Application of photometric models to asteroids. In: Binzel, R.P., Gehrels, T., Matthews, M.S. (Eds.) Asteroids II. Univ. of Arizona Press, Tucson, pp. 524–556.

Bottke, W.F., Vokrouhlický, D., Rubincam, D.P., Nesvorný, D., 2006. The Yarkovsky and YORP effects: Implications for asteroid dynamics. Annu. Rev. Earth Planet. Sci. 34, 157–191.

Carvano, J. M., Barucci, M. A., Fornasier, S., Delbo' M., Lowry, S., and Fitzsimmons, A. 2008. Surface properties of Rosetta's targets (21) Lutetia and (2867)

Steins from ESO observations. Astronomy & Astrophysics, in press.

Christensen, P.R., and 21 colleagues. 2003. Morphology and composition of the surface of Mars: Mars Odyssey THEMIS results. Science, 300, 2056.

Delbo' M., The nature of near-earth asteroids from the study of their thermal infrared emission. 2004. Freie Universitaet Berlin, Digitale Dissertation, on-line at: http://www.diss.fu-berlin.de/2004/289/indexe.html

Delbo', M., Dell'Oro, A., Harris, A. W., Mottola, S., Mueller, M. 2007. Thermal inertia of near-Earth asteroids and implications for the magnitude of the Yarkovsky effect. Icarus 190, 236–249.

Delbo', M., Harris, A. W. 2002. Physical properties of near-Earth asteroids from thermal infrared observations and thermal modeling. Meteoritics and Planetary Science 37, 1929–1936.

Durech, J., Grav, T., Jedicke, R., Denneau, L., Kaasalainen, M. 2005. Asteroid Models from the Pan-STARRS Photometry. Earth, Moon, and Planets 97, 179–187.

Hapke, B., 1984. Bidirectional reflectance spectroscopy. 3. Correction for macroscopic roughness. Icarus 59, 41–59.

Harris, A. W., Mueller, M., Delbo', M., Bus, S. J. 2007. Physical characterization of the potentially hazardous high-albedo Asteroid (33342) 1998 WT_{24} from thermal-infrared observations. Icarus 188, 414–424.

Harris, A. W., Mueller, M., Delbo', M., Bus, S. J. 2005. The surface properties of small asteroids: Peculiar Betulia - A case study. Icarus 179, 95–108.

Jakosky, B. M. 1986. On the thermal properties of Martian fines. Icarus 66, 117–124.

Kaasalainen, M., Mottola, S., Fulchignoni, M. 2002. Asteroid Models from Disk-integrated Data. Asteroids III 139-150.

Kaasalainen, M., Torppa, J., Muinonen, K. 2001. Optimization Methods for Asteroid Lightcurve Inversion. II. The Complete Inverse Problem. Icarus 153, 37-51.

Kaasalainen, M., Torppa, J. 2001. Optimization Methods for Asteroid Lightcurve

Inversion. I. Shape Determination. Icarus 153, 24-36.

Lebofsky, L.A., Spencer, J.R., 1989. Radiometry and thermal modeling of asteroids. In: Binzel, R.P., Gehrels, T., Matthews, M.S. (Eds.), Asteroids II. Univ. of Arizona Press, Tucson, pp. 128–147.

Lebofsky, L. A., Sykes, M. V., Tedesco, E. F., Veeder, G. J., Matson, D. L., Brown, R. H., Gradie, J. C., Feierberg, M. A., Rudy, R. J. 1986. A refined 'standard' thermal model for asteroids based on observations of 1 Ceres and 2 Pallas. Icarus 68, 239–251.

Mellon, M.T., Jakosky, B.M., Kieffer, H.H., Christensen, P.R. 2000. High-resolution thermal inertia mapping from the Mars global surveyor thermal emission spectrometer. Icarus 148, 437–455.

Mignard, F., Cellino, A., Muinonen, K., Tanga, P., Delbo', M., Dell'Oro, A., Granvik, M., Hestroffer, D., Mouret, S., Thuillot, W., Virtanen, J., 2008. The Gaia mission: Expected applications to asteroid science. Earth Moon Planets, 101, 97–125.

Michikami, T., Moriguchi, K., Hasegawa, S., Fujiwara, A. 2007. Ejecta velocity distribution for impact cratering experiments on porous and low strength targets. Planetary and Space Science 55, 70–88.

Morbidelli, A., Vokrouhlický, D., 2003. The Yarkovsky-driven origin of near- Earth asteroids. Icarus 163, 120–134.

Mueller, M. Surface Properties of Asteroids from Mid-Infrared Observations and Thermophysical Modeling. 2007. Freie Universitaet Berlin, Digitale Dissertation, on-line at: http://www.diss.fu-berlin.de/2007/471/indexe.html

Mueller, M., Harris, A.W., Bus, S.J., Hora, J.L., Kassis, M., Adams, J.D. 2006. The size and albedo of Rosetta fly-by target 21 Lutetia from new IRTF measurements and thermal modeling. Astronomy & Astrophysics 447, 1153–1158.

Mueller, M., Delbo', M., di Martino, M., Harris, A.W., Kaasalainen, M., Bus, S.J. submitted in 2004. Indications for regolith on Itokawa from thermal-infrared observations. ASP Conference Series, in press.

Müller, T. G., Sekiguchi, T., Kaasalainen, M., Abe, M., Hasegawa, S. 2005. Thermal infrared observations of the Hayabusa spacecraft target asteroid (25143) Itokawa. Astronomy and Astrophysics 443, 347–355.

Müller, T. G., Sterzik, M. F., Schütz, O., Pravec, P., Siebenmorgen, R. 2004. Thermal infrared observations of near-Earth asteroid 2002 NY40. Astronomy and Astrophysics 424, 1075–1080.

Müller, T. G., Blommaert, J. A. D. L. 2004. 65 Cybele in the thermal infrared: Multiple observations and thermophysical analysis. Astronomy and Astrophysics 418, 347–356.

Müller, T. G., Lagerros, J. S. V. 1998. Asteroids as far-infrared photometric standards for ISOPHOT. Astronomy and Astrophysics 338, 340–352.

Spencer, J. R., Lebofsky, L. A., Sykes, M. V. 1989. Systematic biases in radiometric diameter determinations. Icarus 78, 337–354.

Tedesco, E.F., P.V. Noah, M. Noah, and S.D. Price. 2004. IRAS Minor Planet Survey. IRAS-A-FPA-3-RDR-IMPS-V6.0. NASA Planetary Data System. http://www.psi.edu/pds/resource/imps.html

Tedesco, E.F., Noah, P.V., Noah, M., Price, S.D. 2002. The Supplemental IRAS Minor Planet Survey. Astron. Journal 123, 1056–1085.

Tedesco, E.F. (Ed.) 1992. IRAS Minor Planet Survey. Phillips Laboratory Technical Report No. PL–TR–92–2049. Hanscom Air Force Base, Massachusetts.

Trilling, D. E., Bhattacharya, B., Blaylock, M., Stansberry, J. A., Sykes, M. V., Wasserman, L. H. 2007. The Spitzer Asteroid Catalog: Albedos And Diameters of 35,000 Asteroids. AAS/Division for Planetary Sciences Meeting Abstracts 39, #35.15.

Walsh, K. J., Richardson, D. C. 2006. Binary near-Earth asteroid formation: Rubble pile model of tidal disruptions. Icarus 180, 201–216.

Vokrouhlický, D., Nesvorný, D., Bottke, W. F. 2003. The vector alignments of asteroid spins by thermal torques. Nature 425, 147–151.

Tables and Table Captions

Model	γ_C	ρ_C	$\overline{\theta}$
no roughness	$0°$	0.0	$0°$
low roughness	$45°$	0.5	$10°$
medium roughness	$68°$	0.8	$29°$
high roughness	$90°$	1.0	$58°$

Table 1
The four roughness models used in the application of the TPM to IRAS data. $\overline{\theta}$ is the corresponding mean surface slope according to the parameterization introduced by Hapke (1984) (see text and also Delbo' et al., 2007, for further details)

Number	Designation	H	G	p_V	D (km)	N_s	Dates of observations
21	Lutetia	7.35	0.11	0.221	95.760	20	1983-04-25 → 1983-05-04
32	Pomona	7.56	0.15	0.256	80.760	34	1983-07-31 → 1983-09-05
44	Nysa	7.03	0.46	0.546	70.640	23	1983-07-27 → 1983-09-01
73	Klytia	9.00	0.15	0.225	44.440	26	1983-03-10 → 1983-03-30
110	Lydia	7.80	0.20	0.181	86.090	20	1983-06-25 → 1983-07-03
115	Thyra	7.51	0.12	0.275	79.830	24	1983-04-28 → 1983-05-14
277	Elvira	9.84	0.15	0.277	27.190	19	1983-07-28 → 1983-09-01
306	Unitas	8.96	0.15	0.211	46.700	37	1983-07-31 → 1983-09-07
382	Dodona	8.77	0.15	0.161	58.370	21	1983-07-11 → 1983-08-30
694	Ekard	9.17	0.15	0.046	90.780	35	1983-06-13 → 1983-07-07
720	Bohlinia	9.71	0.15	0.203	33.730	18	1983-08-09 → 1983-09-09

Table 2
Selected main belt asteroids with SIMPS diameters D <100 km, with shape and spin vector solution from lightcurve inversion and a number of IRAS sightings $N_s \geq 20$. H is the absolute magnitude in the $H-G$ system of Bowell et al. (1989) as given in the Minor Planet Center asteroid orbits data base and p_V is the SIPMS geometric visible albedo (Tedesco et al. , 2002). The last column reports the dates of the first and the last IRAS observations.

Number	Designation	Γ J m^{-2} s$^{-0.5}$ K^{-1}	D (km) TPM	p_V TPM	D (km) SIMPS	p_V SIMPS
21	Lutetia	0-100	107-114	0.16-0.18	96 (4)	0.22 (0.02)
32	Pomona	20-120	84-86	0.22-0.24	81 (2)	0.25 (0.01)
44	Nysa	80-160	80-82	0.40-0.42	71 (4)	0.55 (0.07)
110	Lydia	70-200	90-97	0.14-0.16	86 (2)	0.18 (0.01)
115	Thyra	25-100	90-94	0.20-0.22	80 (1)	0.27 (0.01)
277	Elvira	100-400	36-40	0.13-0.16	27 (1)	0.28 (0.02)
306	Unitas	100-260	55-57	0.14-0.15	47 (2)	0.21 (0.02)
382	Dodona	15-150	74-76	0.095-0.10	58 (3)	0.16 (0.02)
694	Ekard	100-140	108-111	0.030-0.032	91 (4)	0.046(0.004)
720	Bohlinia	70-200	40-42	0.13-0.14	34 (1)	0.20 (0.02)

Table 3
Best–fit thermal inertia (Γ) and effective diameters (D) derived from TPM modeling of IRAS data. TPM p_V is derived from the value of the D and the MPC H reported in Tab.2. The quoted uncertainties in diameter and albedo are purely statistical. Systematic uncertainties realted to TPM assumptions are neglected. For comparison we list the SIMPS diameter and geometric visible albedo (p_V) and their quoted uncertainties within parenthesis.

Figure Captions

Figure 1. Thermal inertia as a function of asteroid diameter. Lines with xy–errorbars represent values from the literature. $\times$ with errorbars are the results from this work (see text for details). Dotted line: fit of Eq. (1) to NEAs only; dashed line: fit of Eq. (1) to MBAs only.

Figure 2. Ratio of the diameters derived from thermophysical modeling of IRAS data of the asteroids from this work and their SIMPS diameters, plotted as function of the size of the bodies. Note the inverse correlation of the diameter ratio with size, which may be indicative of the fact the SIMPS size underestimation increases for smaller asteroids.

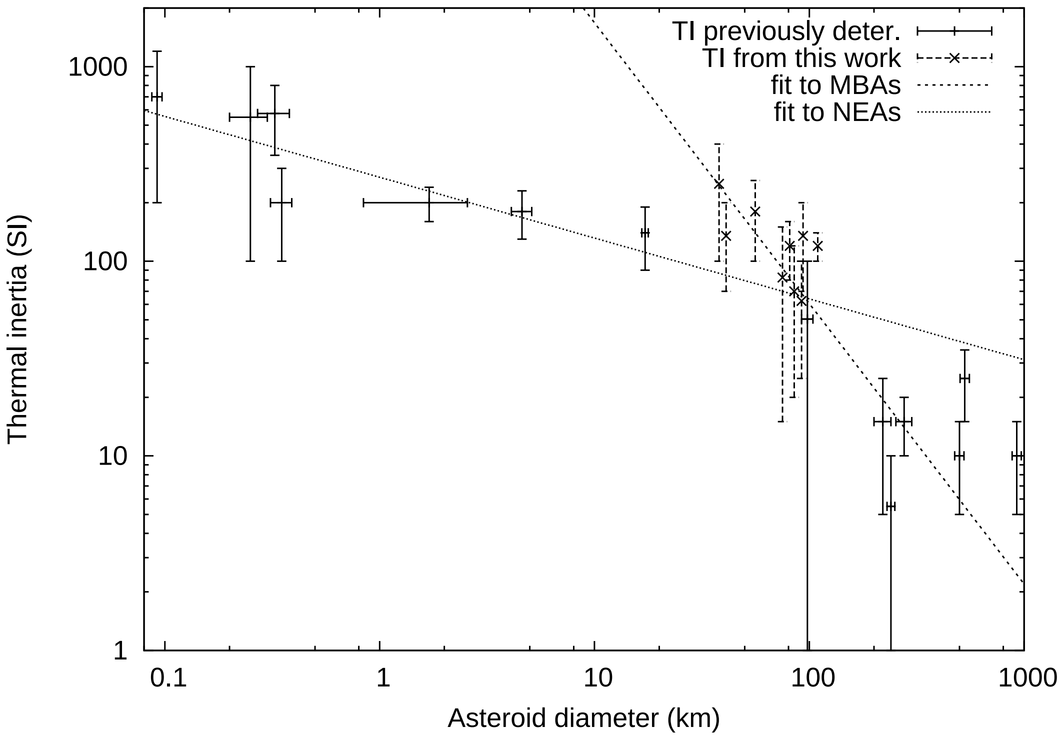
TI previously deter.
TI from this work
fit to MBAs
fit to NEAs
Thermal inertia (SI)
1000
100
10
1
0.1
1
10
100
1000
Asteroid diameter (km)

Fig. 1.

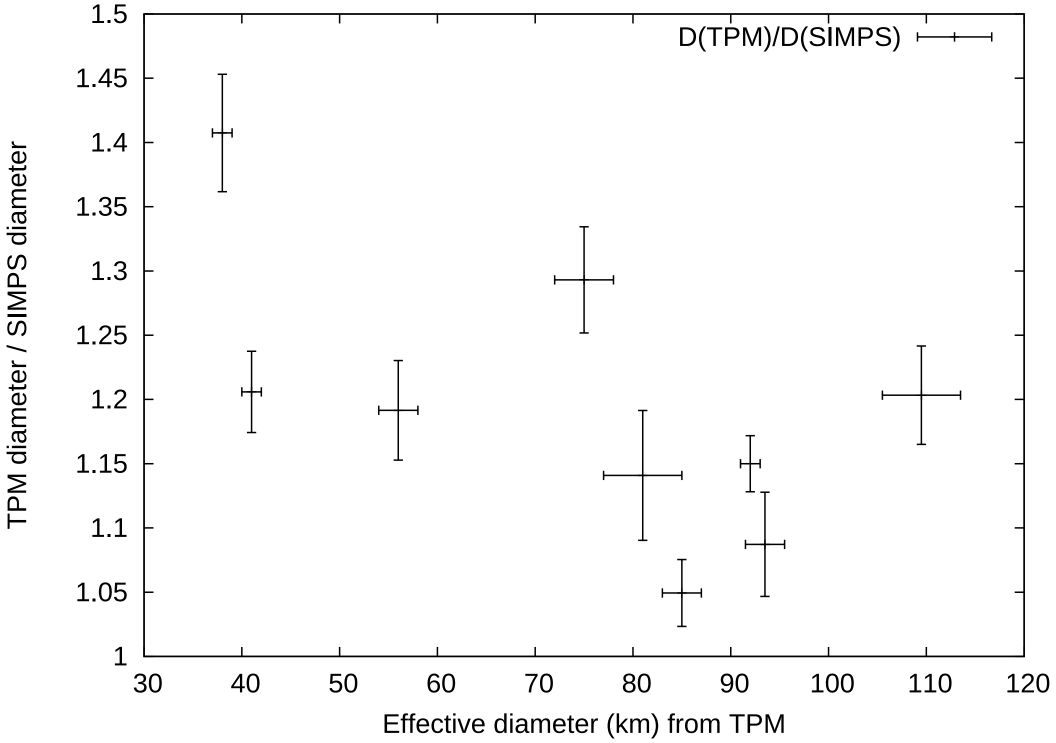
D(TPM)/D(SIMPS)
TPM diameter / SIMPS diameter
1.5
1.45
1.4
1.35
1.3
1.25
1.2
1.15
1.1
1.05
1
30
40
50
60
70
80
90
100
110
120
Effective diameter (km) from TPM

Fig. 2.

Supplementary On–line Material

Description of the TPM results for each target

(21) Lutetia

The model #2 of AMLI (λ_p=217.77°, β_p=12.51°, and P=8.16546082 hrs) gives a lower $\overline{\chi}^2$ for all roughness than the model #1. Thermal inertia ranges from 0 to 180 J m^{-2} s$^{-0.5}$ K^{-1}. The best–fit value of thermal inertia is 90 J m^{-2} s$^{-0.5}$ K^{-1}. The corresponding best–fit D is between 107 and 114 km. Assuming the MPC H=7.35, p_V is in the range between 0.156 and 0.177.

(32) Pomona

A rather high degree of roughness and a thermal inertia between 20 and 220 J m^{-2} s$^{-0.5}$ K^{-1} are admissible solutions. Best fit Γ is 112 J m^{-2} s$^{-0.5}$ K^{-1}. The corresponding best–fit D is 84–86 km, that combined with the MPC H=7.56 yields p_V of 0.22–0.24.

(44) Nysa

The thermal inertia of this object lies in the range between 80 and 160 J m^{-2} s$^{-0.5}$ K^{-1}, with best–fit value of 115 J m^{-2} s$^{-0.5}$ K^{-1}. The degree of surface roughness can not be constrained from the IRAS data. The corresponding best–fit D is between 80 and 82 km that, given then H value of 7.03, yields an albedo p_V of 0.40 – 0.42.

(110) Lydia

Two spin vector and shape model solutions exist for this object. The first (λ_p=149.3°, β_p= -55.0°, P=10.92580365 hrs) gives a slightly better $\overline{\chi}^2$ ($\overline{\chi}^2$=0.7 at Γ=95 J m^{-2} s$^{-0.5}$ K^{-1} on the medium roughness curve) with respect to the second ($\overline{\chi}^2$=0.76 at Γ=120 J m^{-2} s$^{-0.5}$ K^{-1} on the high roughness curve). A thermal inertia between 70 and 200 J m^{-2} s$^{-0.5}$ K^{-1} is also consistent with IRAS data. D range is 90–92 km or 94–97 km depending whether the first of the second pole solution is adopted. Our choice is the first model.

(115) Thyra

Roughness is not constrained for this asteroid, although a surface with a moderate to zero value of roughness is slightly preferred. Nevertheless, if the minima of all roughness model curves are included, we find that thermal inertia varies between 25 and 100 J m^{-2} s$^{-0.5}$ K^{-1}, with a best–fit value of 75 J m^{-2} s$^{-0.5}$ K^{-1}. The best–fit D of this asteroid is between 90 and 94 km, implying an albedo p_V in the range 0.20–0.22 given the H value of 7.51.

(277) Elvira

This object has two shape and spin vector models that provide fits to the IRAS data that are almost indistinguishable. Thermal inertia ranges between

100 and 400 J m^{-2} s$^{-0.5}$ K^{-1}, with a best–fit value Γ=190 J m^{-2} s$^{-0.5}$ K^{-1}, independent of the spin vector solution used. We note that the first model (λ_p=55.99°, β_p=-81.41°, P=29.69216350 hrs) has a marginally lower $\overline{\chi}^2$. The best–fit D ranges from 36 to 40 km, implying a p_V between 0.157 and 0.127 for H=9.84.

(306) Unitas

Two spin vector and shape model solutions are available. The first solution provides a significantly lower $\overline{\chi}^2$ than the second (the value of the $\overline{\chi}^2$ drops by almost a factor of two): we adopt the first solution. The value of the best–fit Γ ranges from 100 to about 260 J m^{-2} s$^{-0.5}$ K^{-1}, with D between 55 and 57 km. Assuming the MPC H value of 8.98 the albedo p_V of this asteroid is between 0.14 and 0.15.

(382) Dodona

Two spin vector and shape model solutions are available. The first one gives a lower $\overline{\chi}^2$ than the second. The best–fit of the second model is obtained is with no roughness: because this is unphysical, we take the first solution as our preferred one. The best–fit thermal inertiais in the range between 15 and 150 J m^{-2} s$^{-0.5}$ K^{-1} and the effective diameter in the range between 74 and 76 km. Assuming the MPC H value of 8.77 the corresponding geometric visible albedo p_V ranges between 0.095 and 0.10.

(694) Ekard

Only one spin vector and shape model from the AMLI exist, and 35 IRAS sightings were acquired. Data at 12, 25, and 60 μm have in general signal to noise ratios of 100 or more. Only the data at 100 μm have lower signal to noise ratios, but none of these <10. Nevertheless, the fit of the TPM to the IRAS data is not very good, with the lowest $\overline{\chi}^2$~4 on the high roughness model at Γ=140 J m^{-2} s$^{-0.5}$ K^{-1}. If the 4 data points at more than 3σ out the TPM predictions are not included in the fit, the minimum of the $\overline{\chi}^2$ drops by almost a factor of 2 ($\overline{\chi}^2$ minimum ~2 at Γ=140 J m^{-2} s$^{-0.5}$ K^{-1} on the high roughness model curve). A thermal inertia between 100 ($\overline{\chi}^2$ minimum on the medium roughness model curve) and 140 J m^{-2} s$^{-0.5}$ K^{-1} provide the best fit to the data. A high level of surface roughness is more consistent with the IRAS data, no matter if the 4 data points at more than 3σ from TPM predictions are included or not in the fit. The best–fit effective diameter ranges from 108 to 111 km and the corresponding value of the geometric visible albedo between 0.030 and 0.032 assuming the MPC H value of 9.17, making this one of the darkest objects observed.

(720) Bohlinia

This object has two shape and spin vector models. The first (λ_p=33.09°, β_p=52.39°, P=8.91861864 hrs) provides a good fit if 100 μm fluxes are removed ($\overline{\chi}^2$=0.8 at Γ=100 J m^{-2} s$^{-0.5}$ K^{-1} on the high roughness model curve and $\overline{\chi}^2$=0.8 at Γ=85 J m^{-2} s$^{-0.5}$ K^{-1} on the medium roughness model curve). For these values of thermal inertia values the effective diameter D ranges between 40 and 42 km and consequently the geometric visible albedo p_V 0.13 and 0.14 assuming the MPC H value of 9.71. Note that the second spin model gives a factor 2 worse fit than the AMLI model #1 to IRAS data, no matter whether the 100 μm fluxes are removed or not. Note that our preferred spin model solution was predicted to be the corrected one just on theoretical grounds (Vokrouhlický et al., 2003, see §4). Vokrouhlický et al. (2003) argued that spins of the four prograde-rotating Koronis asteroids (including Bohlinia) is trapped in a secular spin-orbit resonance which produces their paralelism in space. Our results bring the first observational evidence that this is the case. Note also, that due to very low inclination of the Koronis orbits any optical photometry dataset would not be able to distinguish between the two spin models; it is very interesting that thermophysical modeling of infrared data have the capability to break this degeneracy.

Supplementary On–line Material: Tables

Object	Model	λ_p	β_p	T (h)	ϕ_0	JD_0
21 Lutetia	1	52.72	-5.54	8.16826946	0.0	2444822.351160
	2	217.77	12.51	8.16546082	0.0	2444822.351160
32 Pomona	1	267.07	57.88	9.44766880	0.0	2442747.264590
44 Nysa	1	99.22	57.75	6.42141707	0.0	2433226.633660
73 Klytia	1	38.4	+75.1	8.28306525	0.0	2445831.000000
	2	236.7	+73.4	8.28306625	0.0	2445831.000000
	3	244.18	+13.12	8.29131033	0.0	2445831.000000
110 Lydia	1	149.3	-55.0	10.92580365	0.0	2436494.000000
	2	331.4	-60.9	10.92580271	0.0	2436494.000000
115 Thyra	1	34.52	33.11	7.23996285	0.0	2443845.092510
277 Elvira	1	55.99	-81.41	29.69216350	0.0	2445614.968300
	2	249.37	-79.11	29.69216610	0.0	2445614.968300
306 Unitas	1	79.18	-35.22	8.73874670	0.0	2444113.680260
	2	253.3	-17.4	8.73874674	0.0	2444113.680260
382 Dodona	1	83.03	60.85	4.11322585	0.0	2445412.801460
	2	248.79	54.45	4.11322751	0.0	2445412.801460
694 Ekard	1	88.74	-48.33	5.92200286	0.0	2445590.844030
720 Bohlinia	1	33.09	52.39	8.91861864	0.0	2445467.689780
	2	238.52	39.67	8.91861157	0.0	2445467.689780

Table 4
AMLI spin vector models (downloaded in December 2007) of the asteroids studied in this work. λ_p and β_p are the ecliptic longitude and latitude of the pole, T is the rotation period of the asteroid in hours, ϕ_0 is the absolute rotational phase of the body at the epoch JD_0.

Table 5: Observed IRAS fluxes and quoted uncertainties

Object	Date	Time (UT)	JD	Wavelength (μm)	Flux (Jy)	Error (Jy)
(21) Lutetia						
	1983-04-25	14:10:23	2445450.0905439816	12.0	4.012	0.398
	1983-04-25	14:10:23	2445450.0905439816	25.0	9.989	1.674
	1983-04-25	14:10:23	2445450.0905439816	60.0	5.194	1.139
	1983-04-25	14:10:23	2445450.0905439816	100.0	2.637	0.618
	1983-04-26	00:29:13	2445450.5202893517	12.0	2.974	0.393
	1983-04-26	00:29:13	2445450.5202893517	25.0	7.808	1.156
	1983-04-26	00:29:13	2445450.5202893517	60.0	3.874	0.933
	1983-04-26	00:29:13	2445450.5202893517	100.0	2.146	0.426
	1983-04-26	02:11:59	2445450.5916550928	12.0	3.726	0.430
	1983-04-26	02:11:59	2445450.5916550928	25.0	10.100	1.517
	1983-04-26	02:11:59	2445450.5916550928	60.0	5.425	1.186
	1983-04-26	02:11:59	2445450.5916550928	100.0	1.749	0.314
	1983-05-03	14:32:31	2445458.1059143520	12.0	3.265	0.327
	1983-05-03	14:32:31	2445458.1059143520	25.0	8.813	1.326
	1983-05-03	14:32:31	2445458.1059143520	60.0	4.158	0.902
	1983-05-03	14:32:31	2445458.1059143520	100.0	2.119	0.506
	1983-05-04	00:50:44	2445458.5352314813	12.0	3.159	0.377
	1983-05-04	00:50:44	2445458.5352314813	25.0	9.399	1.574
	1983-05-04	00:50:44	2445458.5352314813	60.0	3.219	0.783
	1983-05-04	00:50:44	2445458.5352314813	100.0	1.568	0.338
(32) Pomona						
	1983-07-31	01:09:28	2445546.5482407408	12.0	2.178	0.268
	1983-07-31	01:09:28	2445546.5482407408	25.0	6.243	0.897
	1983-07-31	01:09:28	2445546.5482407408	60.0	3.561	0.842
	1983-07-31	02:53:41	2445546.6206134260	12.0	1.974	0.260
	1983-07-31	02:53:41	2445546.6206134260	25.0	4.857	0.778
	1983-07-31	02:53:41	2445546.6206134260	60.0	2.659	0.572
	1983-07-31	13:16:15	2445547.0529513890	12.0	2.386	0.287
	1983-07-31	13:16:15	2445547.0529513890	25.0	6.022	0.927
	1983-07-31	13:16:15	2445547.0529513890	60.0	3.354	0.798
	1983-07-31	13:16:15	2445547.0529513890	100.0	1.399	0.253
	1983-08-03	21:58:56	2445550.4159259261	12.0	2.458	0.271
	1983-08-03	21:58:56	2445550.4159259261	25.0	7.156	1.208
	1983-08-03	21:58:56	2445550.4159259261	60.0	2.407	0.551
	1983-08-03	21:58:56	2445550.4159259261	100.0	1.482	0.249
	1983-08-03	23:41:13	2445550.4869560185	12.0	2.423	0.286
	1983-08-03	23:41:13	2445550.4869560185	25.0	6.723	1.050
	1983-08-03	23:41:13	2445550.4869560185	60.0	3.575	0.848
	1983-08-03	23:41:13	2445550.4869560185	100.0	1.085	0.233
	1983-08-11	20:36:42	2445558.3588194447	12.0	2.507	0.286
	1983-08-11	20:36:42	2445558.3588194447	25.0	6.752	1.104
	1983-08-11	20:36:42	2445558.3588194447	60.0	3.274	0.769
	1983-08-11	20:36:42	2445558.3588194447	100.0	1.258	0.252
	1983-08-19	15:47:32	2445566.1580092590	12.0	3.004	0.322
	1983-08-19	15:47:32	2445566.1580092590	25.0	7.544	1.132
	1983-08-19	15:47:32	2445566.1580092590	60.0	4.746	1.130
	1983-08-19	15:47:32	2445566.1580092590	100.0	1.361	0.266
	1983-09-05	20:06:39	2445583.3379513887	12.0	3.951	0.394
	1983-09-05	20:06:39	2445583.3379513887	25.0	10.239	1.521
	1983-09-05	20:06:39	2445583.3379513887	60.0	4.776	1.038
	1983-09-05	20:06:39	2445583.3379513887	100.0	1.771	0.273
	1983-09-05	18:24:29	2445583.2670023148	12.0	3.394	0.353
	1983-09-05	18:24:29	2445583.2670023148	25.0	8.766	1.331
	1983-09-05	18:24:29	2445583.2670023148	60.0	5.049	1.101
	1983-09-05	18:24:29	2445583.2670023148	100.0	1.834	0.314
(44) Nysa						
	1983-07-27	19:54:32	2445543.3295370368	12.0	2.199	0.329
	1983-07-27	19:54:32	2445543.3295370368	25.0	7.315	1.168
	1983-07-27	19:54:32	2445543.3295370368	60.0	2.706	0.636
	1983-07-27	21:37:44	2445543.4012037036	12.0	2.820	0.364
	1983-07-27	21:37:44	2445543.4012037036	25.0	8.113	1.151
	1983-07-27	21:37:44	2445543.4012037036	60.0	3.782	0.818
	1983-07-27	21:37:44	2445543.4012037036	100.0	1.782	0.319
	1983-08-08	18:41:22	2445555.2787268520	12.0	3.415	0.340
	1983-08-08	18:41:22	2445555.2787268520	25.0	9.318	1.571
	1983-08-08	18:41:22	2445555.2787268520	60.0	4.324	1.029
	1983-08-08	18:41:22	2445555.2787268520	100.0	2.041	0.381
	1983-08-08	20:24:25	2445555.3502893518	12.0	2.175	0.289
	1983-08-08	20:24:25	2445555.3502893518	25.0	6.083	1.073
	1983-08-08	20:24:25	2445555.3502893518	60.0	3.075	0.664
	1983-08-08	20:24:25	2445555.3502893518	100.0	1.164	0.250
	1983-09-01	14:48:14	2445579.1168287038	12.0	4.854	0.540

Table 5: Observed IRAS fluxes and quoted uncertainties

Object	Date	Time (UT)	JD	Wavelength (μm)	Flux (Jy)	Error (Jy)
	1983-09-01	14:48:14	2445579.1168287038	25.0	13.025	1.798
	1983-09-01	14:48:14	2445579.1168287038	60.0	6.260	1.376
	1983-09-01	14:48:14	2445579.1168287038	100.0	2.280	0.395
	1983-09-01	16:27:21	2445579.1856597224	12.0	4.001	0.466
	1983-09-01	16:27:21	2445579.1856597224	25.0	11.252	1.658
	1983-09-01	16:27:21	2445579.1856597224	60.0	5.458	1.316
	1983-09-01	16:27:21	2445579.1856597224	100.0	2.147	0.371
(110) Lydia						
	1983-06-25	13:58:32	2445511.0823148149	12.0	2.607	0.373
	1983-06-25	13:58:32	2445511.0823148149	25.0	7.050	1.053
	1983-06-25	13:58:32	2445511.0823148149	60.0	3.989	0.941
	1983-06-25	13:58:32	2445511.0823148149	100.0	0.920	0.188
	1983-06-25	10:32:48	2445510.9394444446	12.0	2.503	0.302
	1983-06-25	10:32:48	2445510.9394444446	25.0	7.412	1.107
	1983-06-25	10:32:48	2445510.9394444446	60.0	4.152	0.996
	1983-06-25	10:32:48	2445510.9394444446	100.0	1.683	0.311
	1983-06-25	12:15:38	2445511.0108564813	12.0	2.325	0.292
	1983-06-25	12:15:38	2445511.0108564813	25.0	6.511	1.083
	1983-06-25	12:15:38	2445511.0108564813	60.0	3.002	0.644
	1983-06-25	12:15:38	2445511.0108564813	100.0	1.576	0.279
	1983-07-03	10:54:18	2445518.9543750002	12.0	2.545	0.438
	1983-07-03	10:54:18	2445518.9543750002	25.0	6.946	1.002
	1983-07-03	10:54:18	2445518.9543750002	60.0	3.604	0.860
	1983-07-03	10:54:18	2445518.9543750002	100.0	1.287	0.258
	1983-07-03	12:37:23	2445519.0259606480	12.0	2.674	0.331
	1983-07-03	12:37:23	2445519.0259606480	25.0	5.515	0.878
	1983-07-03	12:37:23	2445519.0259606480	60.0	3.285	0.703
	1983-07-03	12:37:23	2445519.0259606480	100.0	1.366	0.270
(115) Thyra						
	1983-04-28	02:17:23	2445452.5954050925	12.0	4.881	0.542
	1983-04-28	02:17:23	2445452.5954050925	25.0	9.941	1.676
	1983-04-28	02:17:23	2445452.5954050925	60.0	4.753	1.034
	1983-04-28	02:17:23	2445452.5954050925	100.0	1.793	0.369
	1983-04-28	04:00:52	2445452.6672685184	12.0	4.926	0.566
	1983-04-28	04:00:52	2445452.6672685184	25.0	11.379	1.686
	1983-04-28	04:00:52	2445452.6672685184	60.0	5.302	1.163
	1983-04-28	04:00:52	2445452.6672685184	100.0	2.662	0.591
	1983-05-06	07:54:25	2445460.8294560187	12.0	4.572	0.455
	1983-05-06	07:54:25	2445460.8294560187	25.0	9.601	1.431
	1983-05-06	07:54:25	2445460.8294560187	60.0	4.690	1.021
	1983-05-06	07:54:25	2445460.8294560187	100.0	1.328	0.244
	1983-05-06	09:37:40	2445460.9011574076	12.0	3.922	0.393
	1983-05-06	09:37:40	2445460.9011574076	25.0	9.040	1.507
	1983-05-06	09:37:40	2445460.9011574076	60.0	4.785	1.045
	1983-05-06	09:37:40	2445460.9011574076	100.0	1.433	0.297
	1983-05-14	11:43:54	2445468.9888194446	12.0	3.949	0.421
	1983-05-14	11:43:54	2445468.9888194446	25.0	8.612	1.412
	1983-05-14	11:43:54	2445468.9888194446	60.0	3.801	0.827
	1983-05-14	11:43:54	2445468.9888194446	100.0	1.769	0.368
	1983-05-14	13:27:14	2445469.0605787039	12.0	3.506	0.352
	1983-05-14	13:27:14	2445469.0605787039	25.0	7.789	1.317
	1983-05-14	13:27:14	2445469.0605787039	60.0	3.926	0.926
	1983-05-14	13:27:14	2445469.0605787039	100.0	1.911	0.407
(277) Elvira						
	1983-07-28	13:13:19	2445544.0509143518	12.0	0.436	0.082
	1983-07-28	13:13:19	2445544.0509143518	25.0	1.144	0.231
	1983-07-28	13:13:19	2445544.0509143518	60.0	0.669	0.145
	1983-07-28	13:13:19	2445544.0509143518	100.0	1.446	0.316
	1983-07-28	14:49:54	2445544.1179861110	12.0	0.507	0.093
	1983-07-28	14:49:54	2445544.1179861110	25.0	0.939	0.215
	1983-07-28	14:49:54	2445544.1179861110	60.0	0.593	0.112
	1983-08-08	23:51:54	2445555.4943749998	12.0	0.447	0.082
	1983-08-08	23:51:54	2445555.4943749998	25.0	0.948	0.196
	1983-08-08	23:51:54	2445555.4943749998	60.0	0.561	0.106
	1983-08-09	01:34:53	2445555.5658912039	12.0	0.352	0.068
	1983-08-09	01:34:53	2445555.5658912039	25.0	0.849	0.175
	1983-08-09	01:34:53	2445555.5658912039	60.0	0.637	0.136
	1983-09-01	14:49:41	2445579.1178356484	12.0	0.541	0.090
	1983-09-01	14:49:41	2445579.1178356484	25.0	1.543	0.282
	1983-09-01	14:49:41	2445579.1178356484	60.0	0.819	0.157
	1983-09-01	16:28:48	2445579.1866666665	12.0	0.615	0.098
	1983-09-01	16:28:48	2445579.1866666665	25.0	1.702	0.304
	1983-09-01	16:28:48	2445579.1866666665	60.0	0.753	0.149
(306) Unitas						

Table 5: Observed IRAS fluxes and quoted uncertainties

Object	Date	Time (UT)	JD	Wavelength (μm)	Flux (Jy)	Error (Jy)
	1983-07-31	02:51:32	2445546.6191203706	12.0	3.490	0.441
	1983-07-31	02:51:32	2445546.6191203706	25.0	5.988	0.883
	1983-07-31	02:51:32	2445546.6191203706	60.0	2.619	0.619
	1983-07-31	01:07:19	2445546.5467476854	12.0	2.521	0.321
	1983-07-31	01:07:19	2445546.5467476854	25.0	4.683	0.747
	1983-07-31	01:07:19	2445546.5467476854	60.0	2.331	0.552
	1983-07-31	13:14:06	2445547.0514583332	12.0	2.328	0.327
	1983-07-31	13:14:06	2445547.0514583332	25.0	4.753	0.673
	1983-07-31	13:14:06	2445547.0514583332	60.0	2.004	0.473
	1983-08-04	01:21:10	2445550.5563657410	12.0	2.214	0.259
	1983-08-04	01:21:10	2445550.5563657410	25.0	4.760	0.666
	1983-08-04	01:21:10	2445550.5563657410	60.0	2.378	0.562
	1983-08-03	23:39:01	2445550.4854282406	12.0	2.998	0.310
	1983-08-03	23:39:01	2445550.4854282406	25.0	5.569	0.787
	1983-08-03	23:39:01	2445550.4854282406	60.0	2.657	0.628
	1983-08-12	15:28:44	2445559.1449537035	12.0	3.057	0.305
	1983-08-12	15:28:44	2445559.1449537035	25.0	5.737	0.930
	1983-08-12	15:28:44	2445559.1449537035	60.0	2.640	0.566
	1983-08-12	13:47:29	2445559.0746412035	12.0	2.761	0.312
	1983-08-12	13:47:29	2445559.0746412035	25.0	5.133	0.827
	1983-08-12	13:47:29	2445559.0746412035	60.0	2.574	0.548
	1983-08-20	15:48:60	2445567.1590277776	12.0	3.495	0.348
	1983-08-20	15:48:60	2445567.1590277776	25.0	7.034	1.050
	1983-08-20	15:48:60	2445567.1590277776	60.0	3.350	0.788
	1983-08-20	15:48:60	2445567.1590277776	100.0	1.882	0.318
	1983-08-20	17:32:12	2445567.2306944444	12.0	3.166	0.348
	1983-08-20	17:32:12	2445567.2306944444	25.0	6.159	1.008
	1983-08-20	17:32:12	2445567.2306944444	60.0	2.718	0.581
	1983-08-20	17:32:12	2445567.2306944444	100.0	2.199	0.430
	1983-09-07	21:53:22	2445585.4120601853	12.0	4.294	0.466
	1983-09-07	21:53:22	2445585.4120601853	25.0	9.710	1.596
	1983-09-07	21:53:22	2445585.4120601853	60.0	2.987	0.707
	1983-09-07	21:53:22	2445585.4120601853	100.0	2.218	0.417
	1983-09-07	23:36:27	2445585.4836458336	12.0	3.929	0.391
	1983-09-07	23:36:27	2445585.4836458336	25.0	8.472	1.247
	1983-09-07	23:36:27	2445585.4836458336	60.0	3.968	0.942
	1983-09-07	23:36:27	2445585.4836458336	100.0	2.588	0.511
(382) Dodona						
	1983-07-11	11:21:47	2445526.9734606482	12.0	1.554	0.208
	1983-07-11	11:21:47	2445526.9734606482	25.0	4.083	0.570
	1983-07-11	11:21:47	2445526.9734606482	60.0	2.515	0.594
	1983-07-11	11:21:47	2445526.9734606482	100.0	1.002	0.204
	1983-07-11	13:04:52	2445527.0450462964	12.0	2.173	0.261
	1983-07-11	13:04:52	2445527.0450462964	25.0	5.039	0.706
	1983-07-11	13:04:52	2445527.0450462964	60.0	2.316	0.495
	1983-07-11	13:04:52	2445527.0450462964	100.0	1.481	0.333
	1983-07-23	08:32:23	2445538.8558217594	12.0	2.092	0.319
	1983-07-23	08:32:23	2445538.8558217594	25.0	5.110	0.798
	1983-07-23	08:32:23	2445538.8558217594	60.0	2.815	0.669
	1983-07-23	10:15:39	2445538.9275347223	12.0	2.051	0.290
	1983-07-23	10:15:39	2445538.9275347223	25.0	5.334	0.854
	1983-07-23	10:15:39	2445538.9275347223	60.0	1.927	0.453
	1983-07-23	10:15:39	2445538.9275347223	100.0	1.059	0.193
	1983-08-30	06:59:28	2445576.7912962963	12.0	1.222	0.179
	1983-08-30	06:59:28	2445576.7912962963	25.0	3.274	0.543
	1983-08-30	06:59:28	2445576.7912962963	60.0	1.506	0.297
	1983-08-30	08:42:35	2445576.8629050925	12.0	1.276	0.201
	1983-08-30	08:42:35	2445576.8629050925	25.0	3.165	0.553
	1983-08-30	08:42:35	2445576.8629050925	60.0	1.650	0.341
(694) Ekard						
	1983-06-13	22:52:16	2445499.4529629629	12.0	24.364	2.842
	1983-06-13	22:52:16	2445499.4529629629	25.0	32.217	3.317
	1983-06-13	22:52:16	2445499.4529629629	60.0	13.672	2.824
	1983-06-13	22:52:16	2445499.4529629629	100.0	3.947	0.858
	1983-06-14	00:34:56	2445499.5242592595	12.0	26.906	3.291
	1983-06-14	00:34:56	2445499.5242592595	25.0	43.510	4.489
	1983-06-14	00:34:56	2445499.5242592595	60.0	15.685	3.743
	1983-06-14	00:34:56	2445499.5242592595	100.0	6.844	1.497
	1983-06-13	21:09:33	2445499.3816319443	12.0	25.625	3.058
	1983-06-13	21:09:33	2445499.3816319443	25.0	38.516	3.970
	1983-06-13	21:09:33	2445499.3816319443	60.0	18.138	4.659
	1983-06-13	21:09:33	2445499.3816319443	100.0	4.553	0.914
	1983-06-23	14:48:24	2445509.1169444444	12.0	23.688	2.914
	1983-06-23	14:48:24	2445509.1169444444	25.0	35.971	3.991

Table 5: Observed IRAS fluxes and quoted uncertainties

Object	Date	Time (UT)	JD	Wavelength (μm)	Flux (Jy)	Error (Jy)
	1983-06-23	14:48:24	2445509.1169444444	60.0	15.918	3.319
	1983-06-23	14:48:24	2445509.1169444444	100.0	4.604	1.127
	1983-06-23	16:31:40	2445509.1886574072	12.0	27.770	3.704
	1983-06-23	16:31:40	2445509.1886574072	25.0	38.734	3.992
	1983-06-23	16:31:40	2445509.1886574072	60.0	18.129	4.385
	1983-06-23	16:31:40	2445509.1886574072	100.0	5.715	1.265
	1983-06-23	18:14:53	2445509.2603356480	12.0	30.152	3.589
	1983-06-23	18:14:53	2445509.2603356480	25.0	47.105	4.862
	1983-06-23	18:14:53	2445509.2603356480	60.0	17.334	3.990
	1983-06-23	18:14:53	2445509.2603356480	100.0	6.954	1.698
	1983-07-07	15:29:12	2445523.1452777777	12.0	31.737	3.140
	1983-07-07	15:29:12	2445523.1452777777	25.0	48.717	5.029
	1983-07-07	15:29:12	2445523.1452777777	60.0	17.682	4.059
	1983-07-07	15:29:12	2445523.1452777777	100.0	7.714	1.889
	1983-07-07	05:17:52	2445522.7207407407	12.0	17.712	1.904
	1983-07-07	05:17:52	2445522.7207407407	25.0	55.794	5.766
	1983-07-07	05:17:52	2445522.7207407407	60.0	23.059	6.503
	1983-07-07	05:17:52	2445522.7207407407	100.0	9.138	2.025
	1983-07-07	13:45:56	2445523.0735648149	12.0	33.854	4.502
	1983-07-07	13:45:56	2445523.0735648149	25.0	56.635	5.853
	1983-07-07	13:45:56	2445523.0735648149	100.0	7.475	1.607
(720) Bohlinia						
	1983-08-09	07:41:37	2445555.8205671296	12.0	0.562	0.111
	1983-08-09	07:41:37	2445555.8205671296	25.0	1.520	0.329
	1983-08-09	07:41:37	2445555.8205671296	60.0	0.445	0.089
	1983-08-09	05:58:41	2445555.7490856480	12.0	0.349	0.058
	1983-08-09	05:58:41	2445555.7490856480	25.0	1.249	0.254
	1983-08-09	05:58:41	2445555.7490856480	60.0	0.672	0.124
	1983-08-09	05:58:41	2445555.7490856480	100.0	1.280	0.223
	1983-08-21	03:03:08	2445567.6271759258	12.0	0.429	0.072
	1983-08-21	03:03:08	2445567.6271759258	25.0	1.268	0.292
	1983-08-21	03:03:08	2445567.6271759258	60.0	0.547	0.114
	1983-08-21	06:29:16	2445567.7703240742	25.0	1.147	0.230
	1983-08-21	06:29:16	2445567.7703240742	60.0	0.581	0.108
	1983-08-21	04:46:11	2445567.6987384260	12.0	0.380	0.062
	1983-08-21	04:46:11	2445567.6987384260	25.0	1.056	0.234
	1983-08-21	04:46:11	2445567.6987384260	60.0	0.572	0.104
	1983-09-09	10:51:47	2445586.9526273147	12.0	0.309	0.053
	1983-09-09	10:51:47	2445586.9526273147	25.0	1.227	0.281
	1983-09-09	10:51:47	2445586.9526273147	60.0	0.473	0.088

Supplementary On–line Material: Figures and Figure Captions

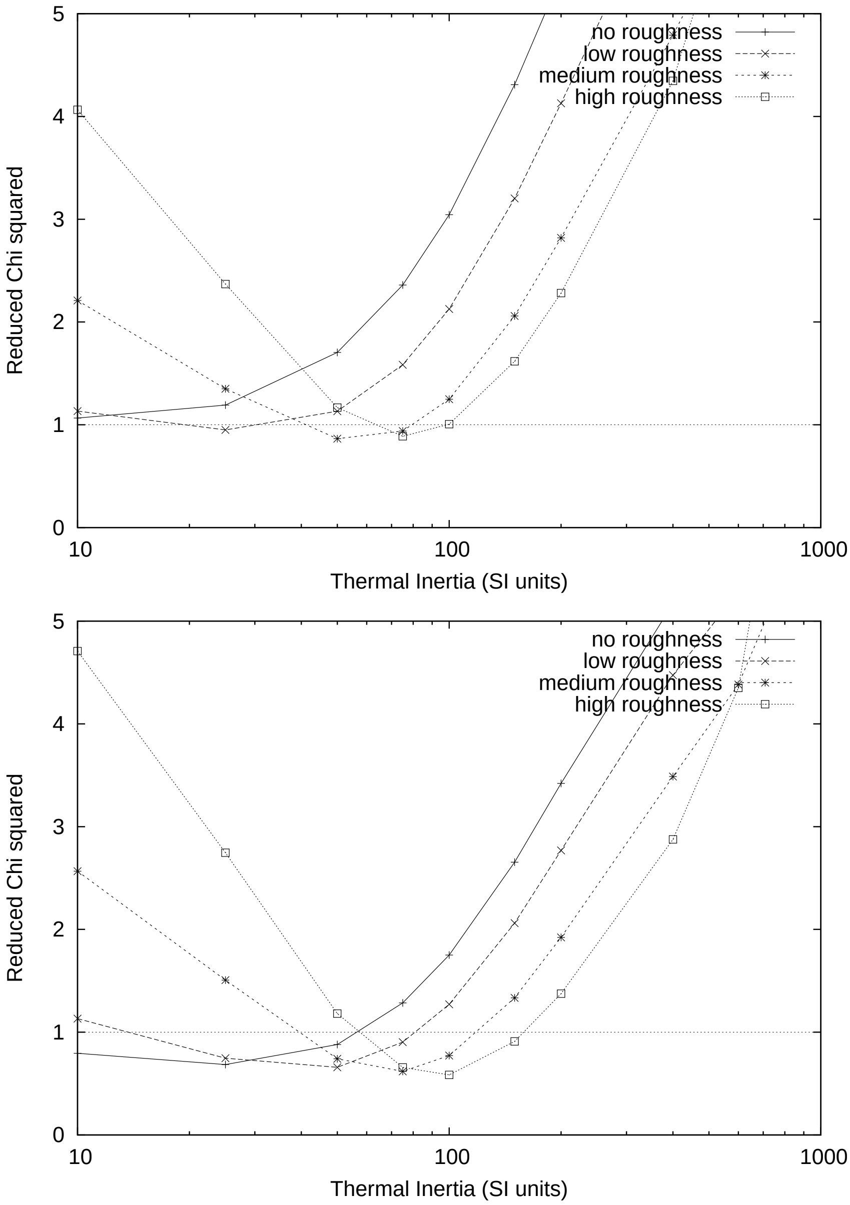

Fig. 3. Reduced $\overline{\chi}^2$ of the TPM fit to IRAS infrared data as function of the thermal inertia for the asteroid (21) Lutetia. See §2 for the definition of the $\overline{\chi}^2$ adopted in this work. Each curve corresponds to a different roughness model (see the legend on the top right of the plot and Table 1). The best–fit thermal inertia is the abscissa of the minimum $\overline{\chi}^2$. An horizontal line is drawn at $\overline{\chi}^2$=1. Admissible solution values for thermal inertia and surface roughness are defined by that portion of the curves with $\overline{\chi}^2 \leq 1$. Top: AMLI shape and spin vector solution 1, bottom: AMLI solution 2

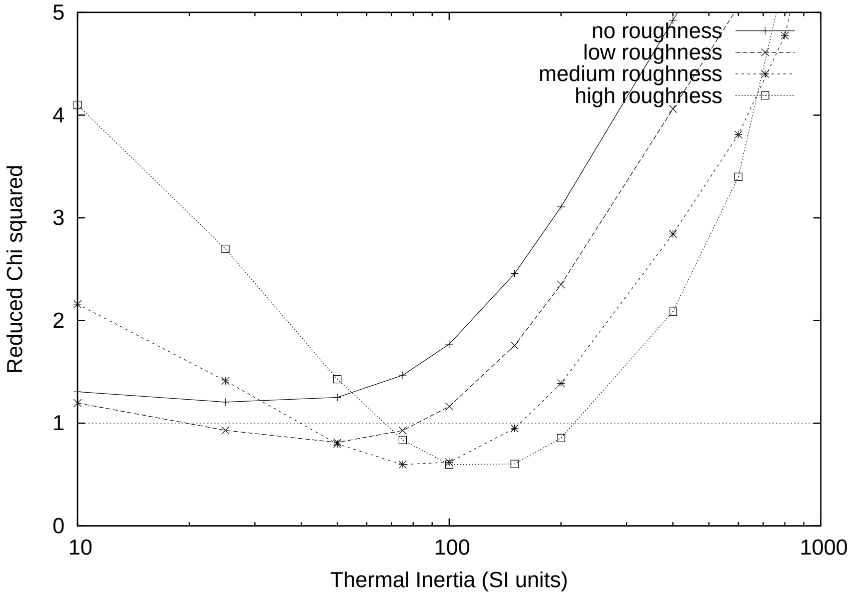

Fig. 4. As of Fig. 3 but for the asteroid (32) Pomona.

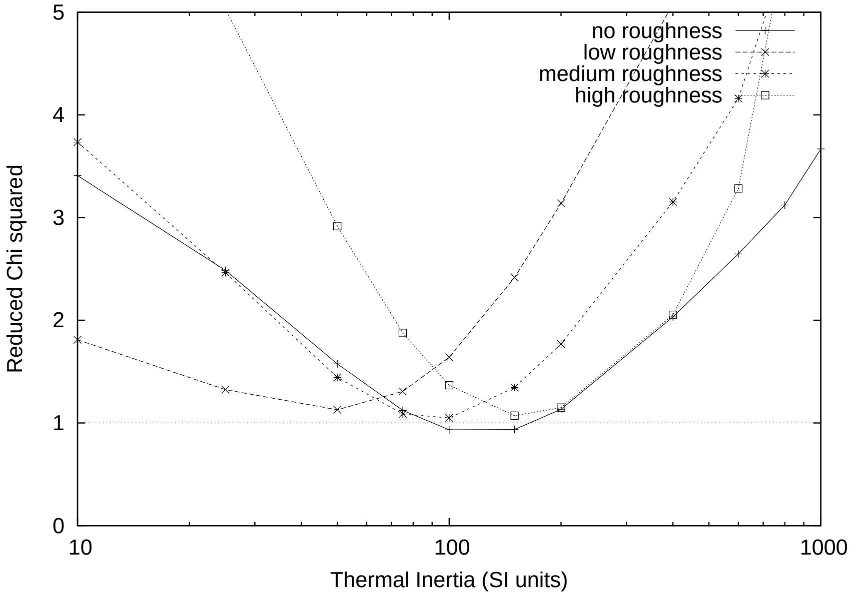

Fig. 5. As of Fig. 3 but for the asteroid (44) Nysa.

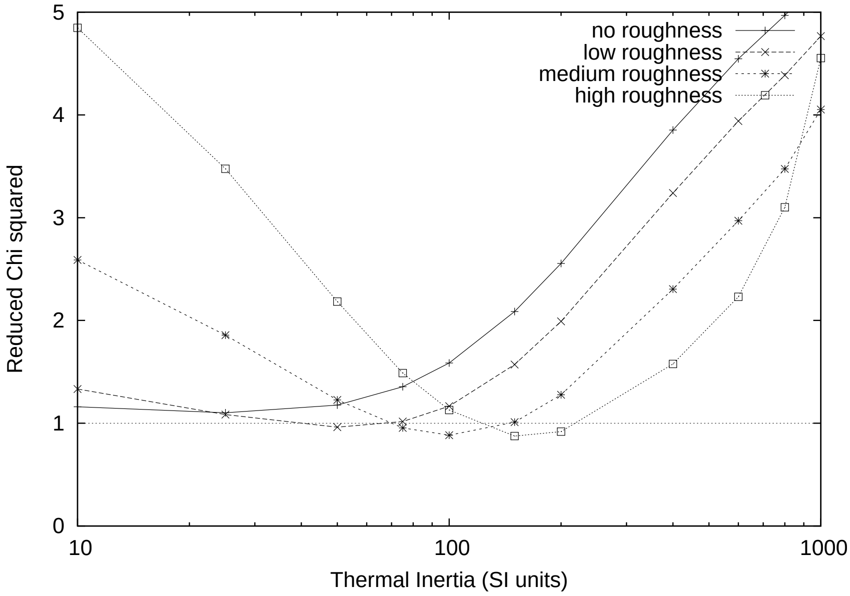

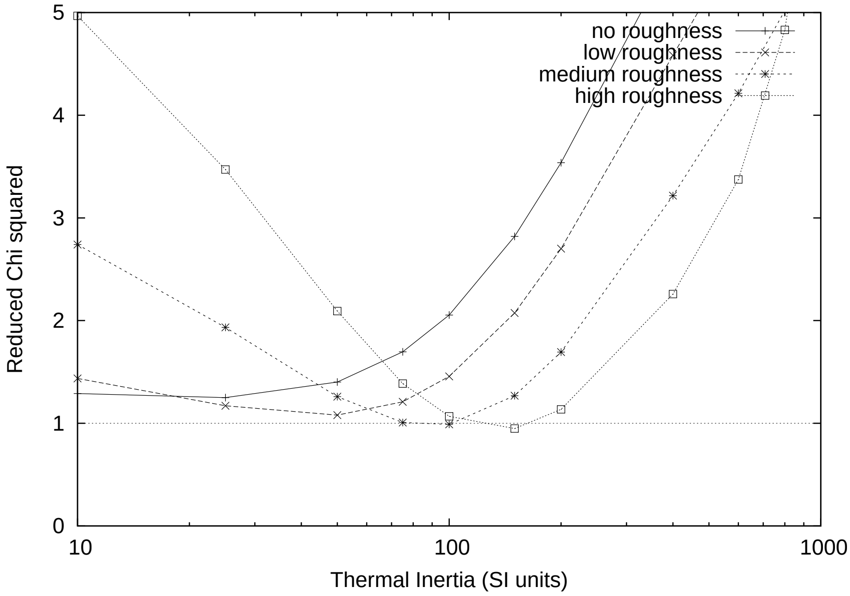

Fig. 6. As of Fig. 3 but for the asteroid (110) Lydia. Top: AMLI shape and spin vector solution 1, bottom: AMLI solution 2

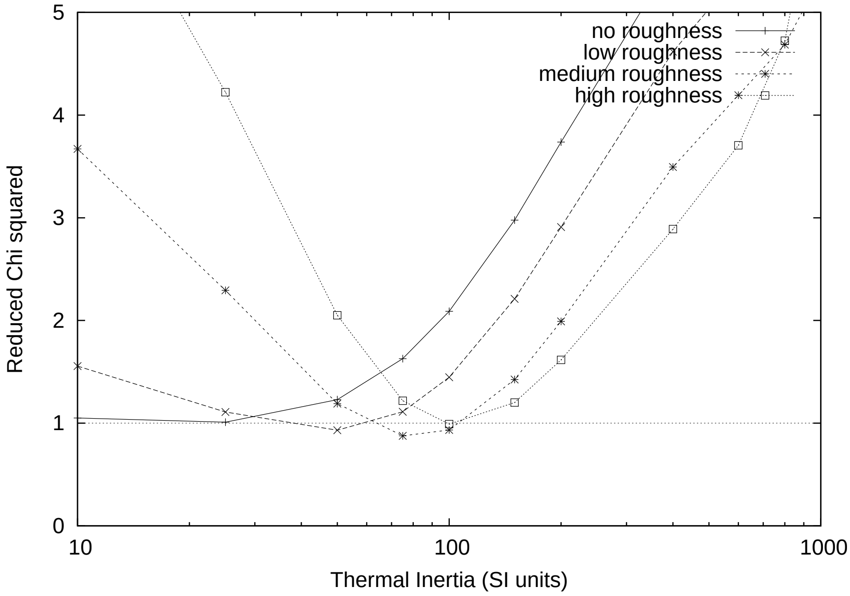

Fig. 7. As of Fig. 3 but for the asteroid (115) Thyra.

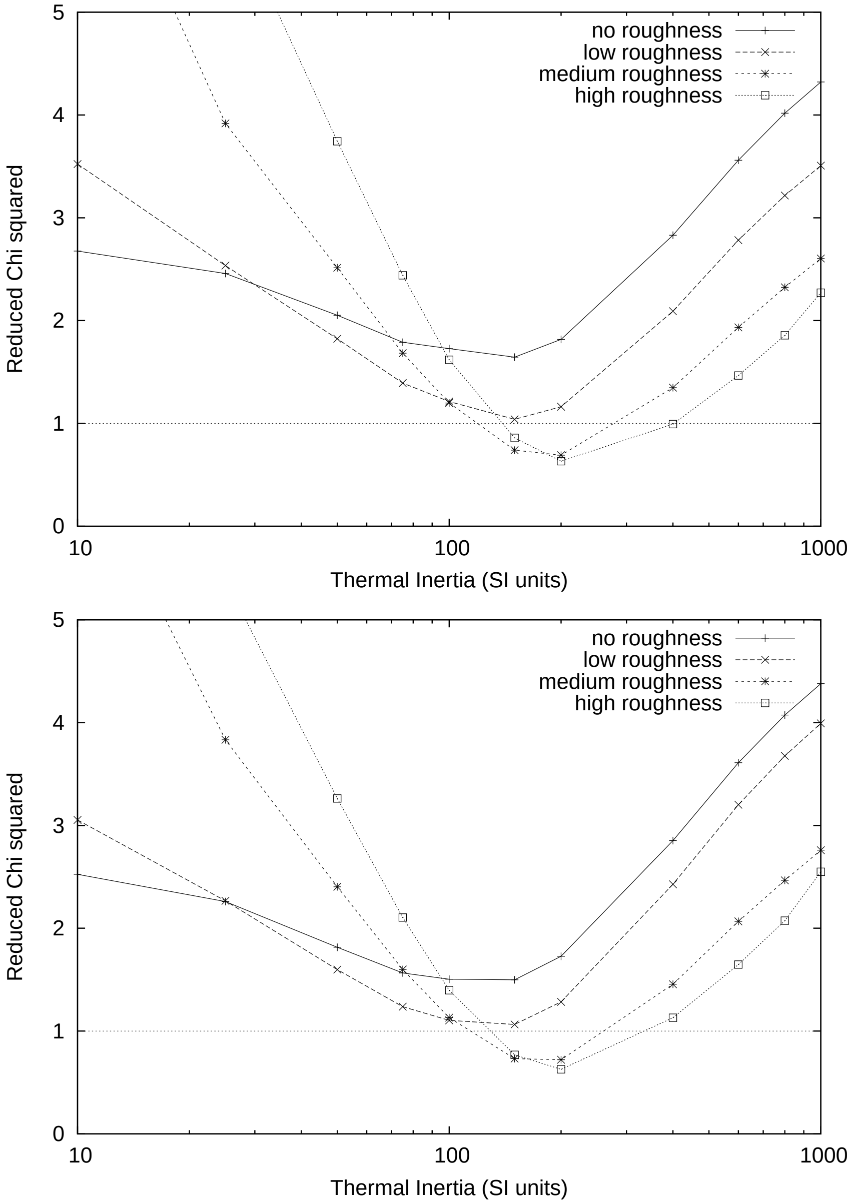

Fig. 8. As of Fig. 3 but for the asteroid (277) Elvira. Top: AMLI shape and spin vector solution 1, bottom: AMLI solution 2.

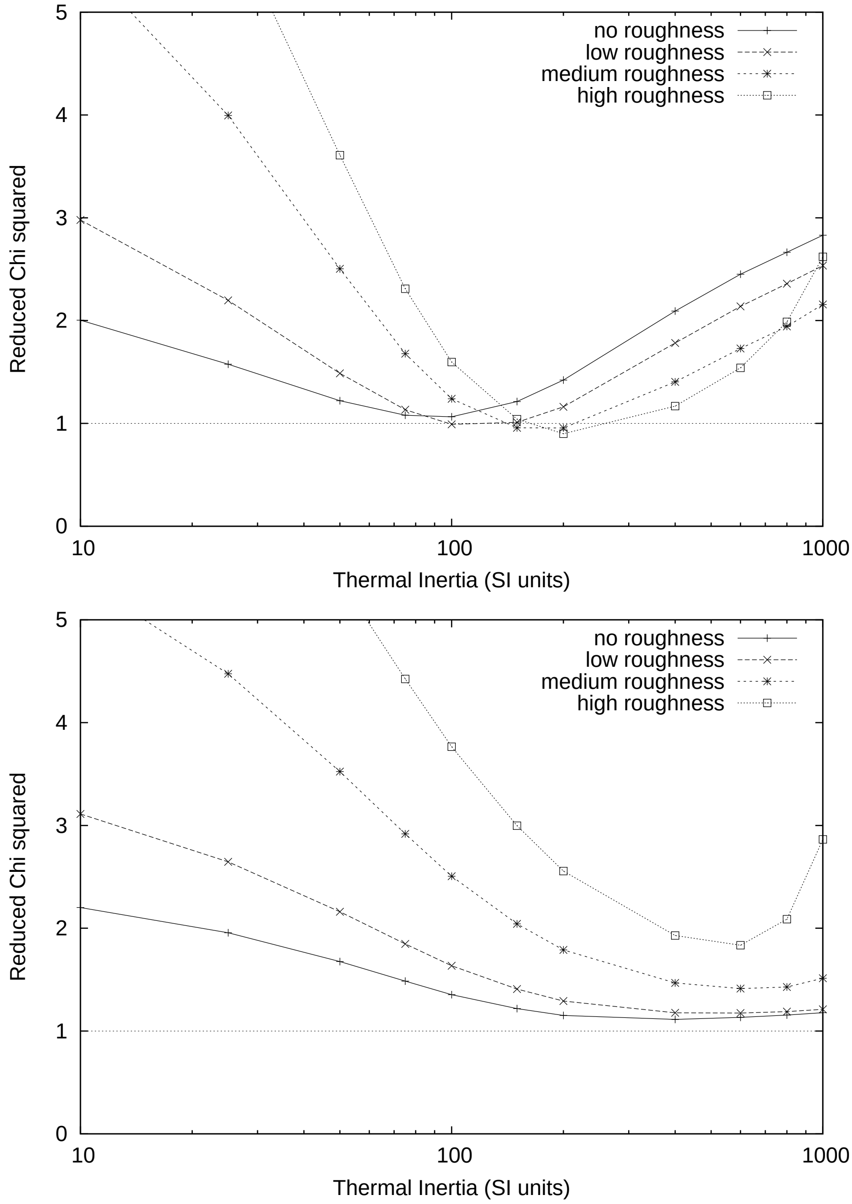

Fig. 9. As of Fig. 3 but for the asteroid (306) Unitas. Top: AMLI shape and spin vector solution 1, bottom: AMLI solution 2.

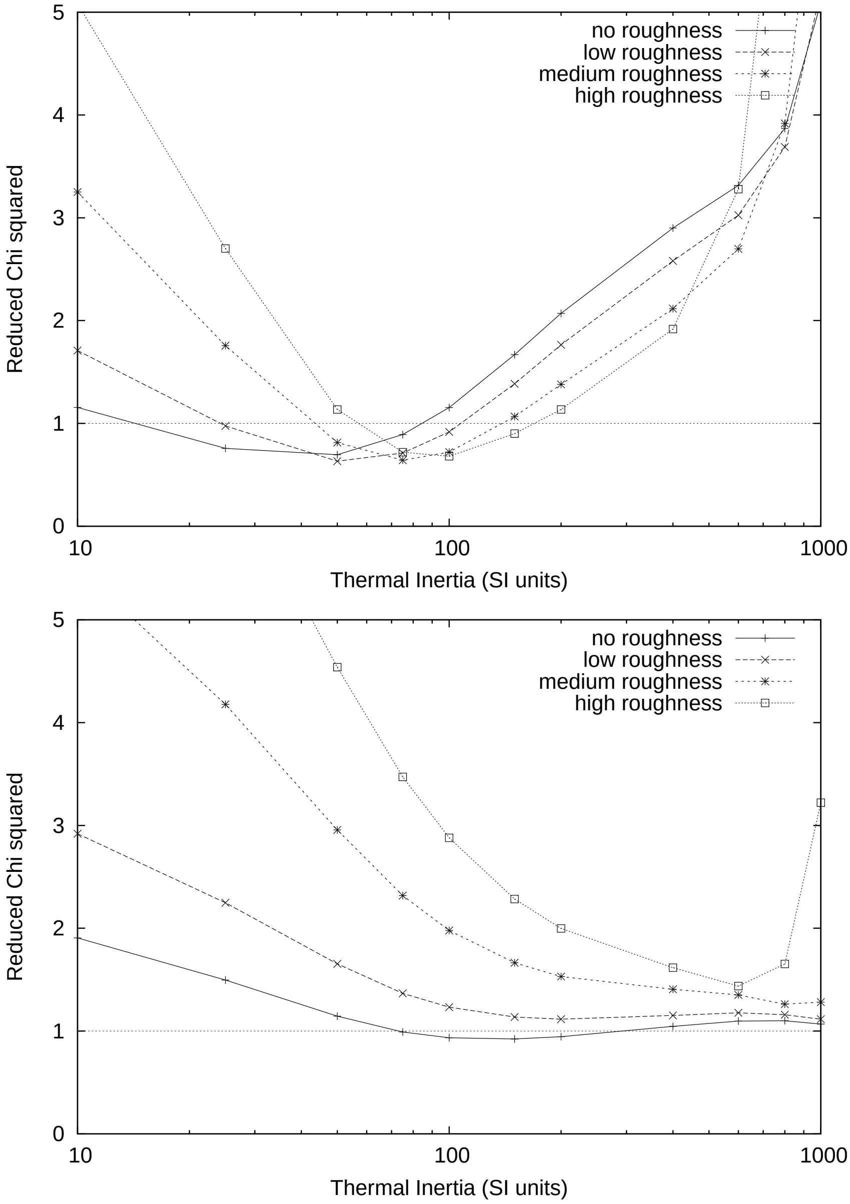

Fig. 10. As of Fig. 3 but for the asteroid (382) Dodona. Top: AMLI shape and spin vector solution 1, bottom: AMLI solution 2.

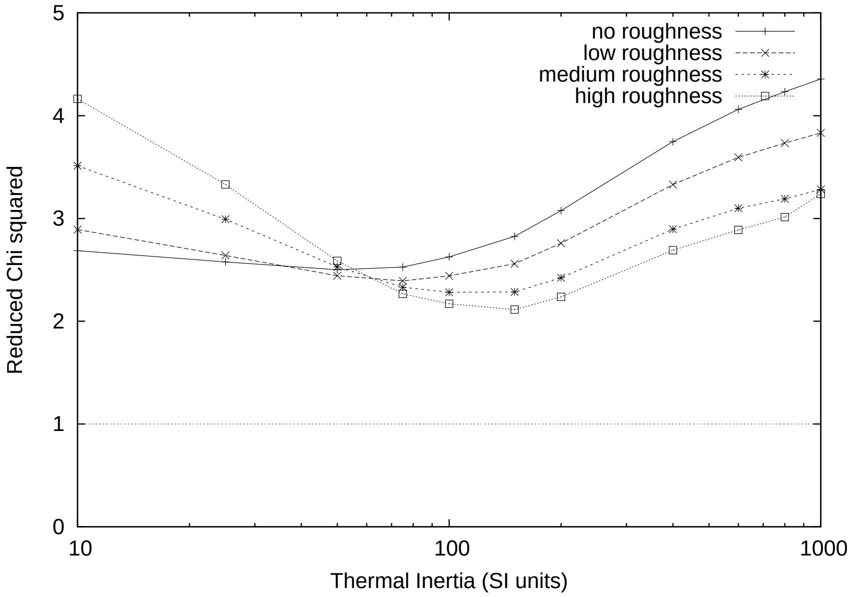

Fig. 11. As of Fig. 3 but for the asteroid (694) Ekard.

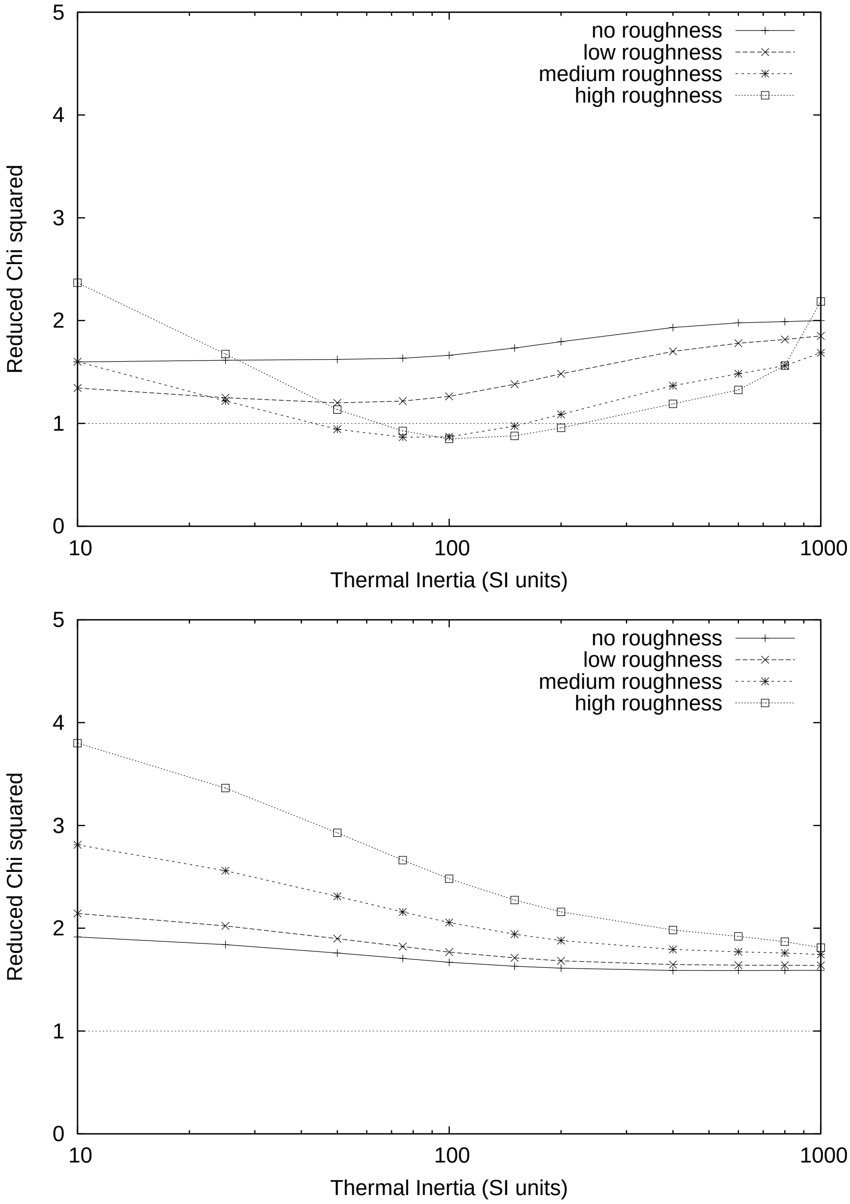

Fig. 12. As of Fig. 3 but for the asteroid (720) Bohlinia. Top: AMLI shape and spin vector solution 1, bottom: AMLI solution 2.